

Exploring Dual-Iron Atomic Catalysts for Efficient Nitrogen Reduction: A Comprehensive Study on Structural and Electronic Optimization

Zhe Zhang^a, Wenxin Ma^a, Jiajie Qiao^a, Xiaoliang Wu^a, Shaowen Yu^a, Weiye Hou^a, Xiang Huang^a,
Rubin Huo^a, Hongbo Wu^{*,b,c} and Yusong Tu^{*,a}

^aCollege of Physics Science and Technology, Yangzhou University, Jiangsu 225009, China

^bSchool of Science, Yangzhou Polytechnic Institute, Yangzhou 225127, China

^cCollege of Physics, Hebei Normal University, Shijiazhuang 050024, China

*Corresponding Authors: zzhang@yzu.edu.cn; wuhb@ypi.edu.cn; ystu@yzu.edu.cn

1. Computational methods

To investigate the thermodynamic and electrochemical stability, we calculate the formation energy (E_f) and dissolution potential (U_{diss}) of the TM-anchored graphene. The E_f and U_{diss} of $\text{Fe}_2\text{N}_x\text{B}_y@\text{G}$, $\text{Fe}_2\text{N}_x\text{O}_y@\text{G}$ and $\text{Fe}_2\text{N}_x\text{S}_y@\text{G}$ systems are defined as

$$E_f = (E_{2\text{TM}/\text{sub}} - E_{\text{sub}} - 2E_{\text{TM}})/2, \quad (1)$$

$$U_{\text{diss}} = U_{\text{diss}}^{\circ}(\text{metal,bulk}) - E_f/n'e \quad (2)$$

where $E_{2\text{TM}/\text{sub}}$ are the total energies of $\text{Fe}_2\text{N}_x\text{B}_y@\text{G}$, $\text{Fe}_2\text{N}_x\text{O}_y@\text{G}$ and $\text{Fe}_2\text{N}_x\text{S}_y@\text{G}$ systems. E_{sub} and E_{TM} are the total energies of substrate and single transition metal atom energy in its most stable bulk structure, respectively. n' is the number of transferred electrons, and $U_{\text{diss}}^{\circ}(\text{metal, bulk})$ is the standard dissolution potential of bulk metal in the dissolution process.

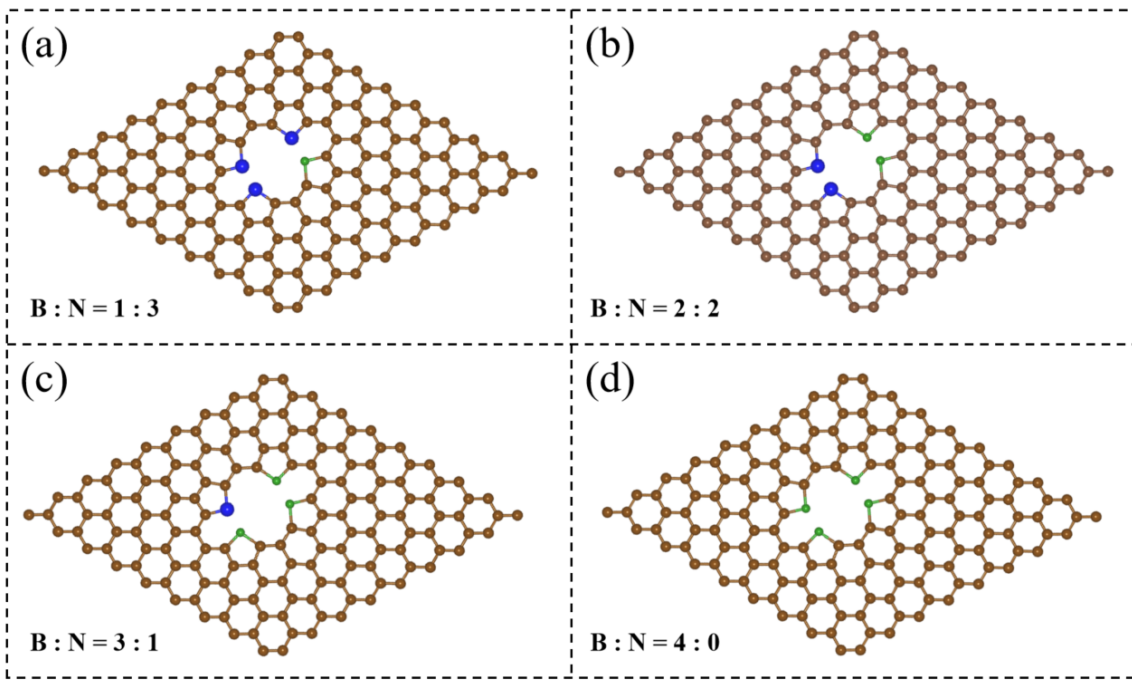


Figure S1. Structural models of the graphene sheets with different B:N doping ratios. (a) B:N = 1:3, (b) B:N = 2:2, (c) B:N = 3:1, (d) B:N = 4:0. The blue, green and brown balls represent nitrogen, boron and carbon atoms, respectively.

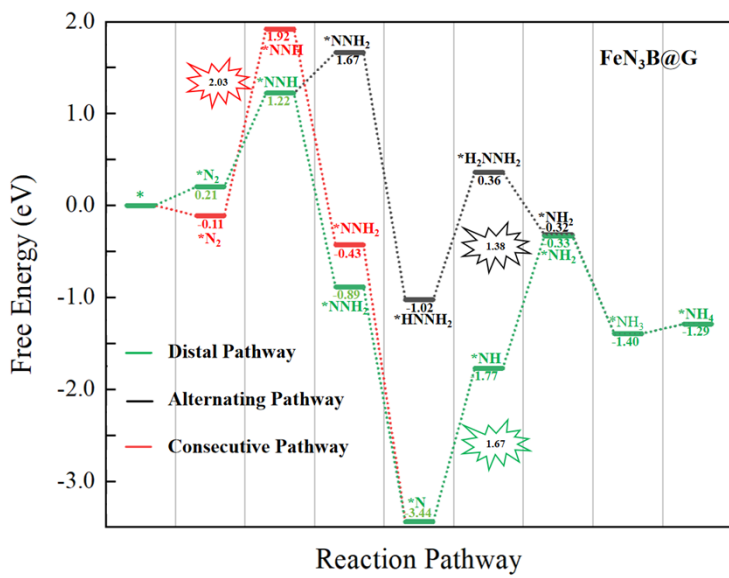


Figure S2. Free energy profiles of NRR on FeN₃B@G catalyst.

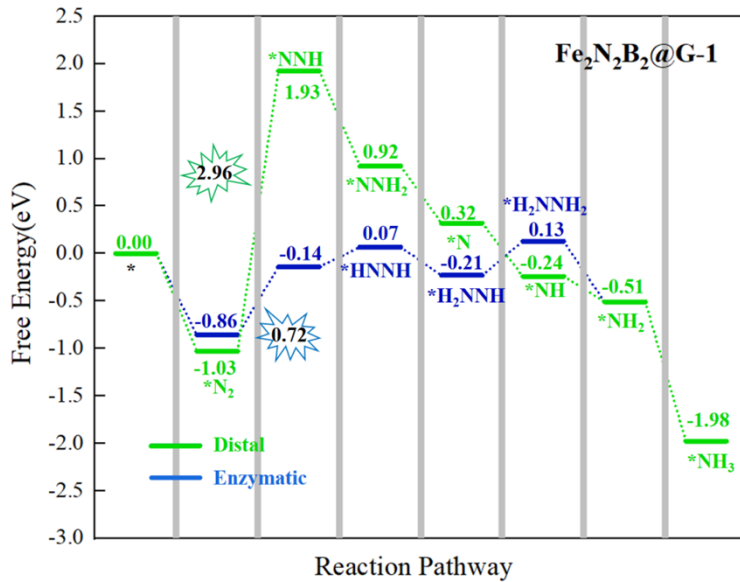


Figure S3. Free energy changes of a centrosymmetric $\text{Fe}_2\text{N}_2\text{B}_2@\text{G-1}$ structure with a B:N doping ratio of 2:2.

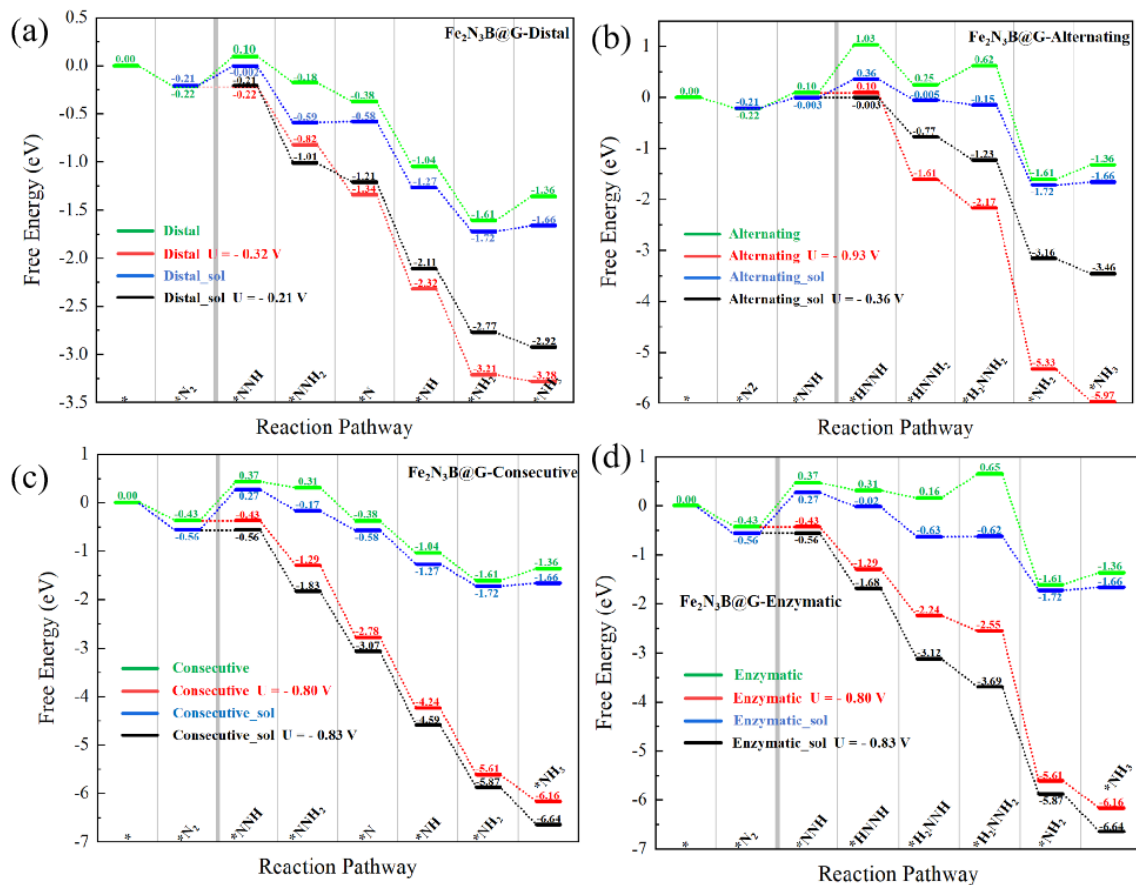


Figure S4. Free energy profiles of $\text{Fe}_2\text{N}_3\text{B}@\text{G}$ catalyst for NRR under different pathways: (a) distal, (b) alternating, (c) consecutive, and (d) enzymatic. Each panel shows the standard pathway (green), the pathway under applied potential (red), with solvation effect (blue), and with both solvation and applied potential corrections (black).

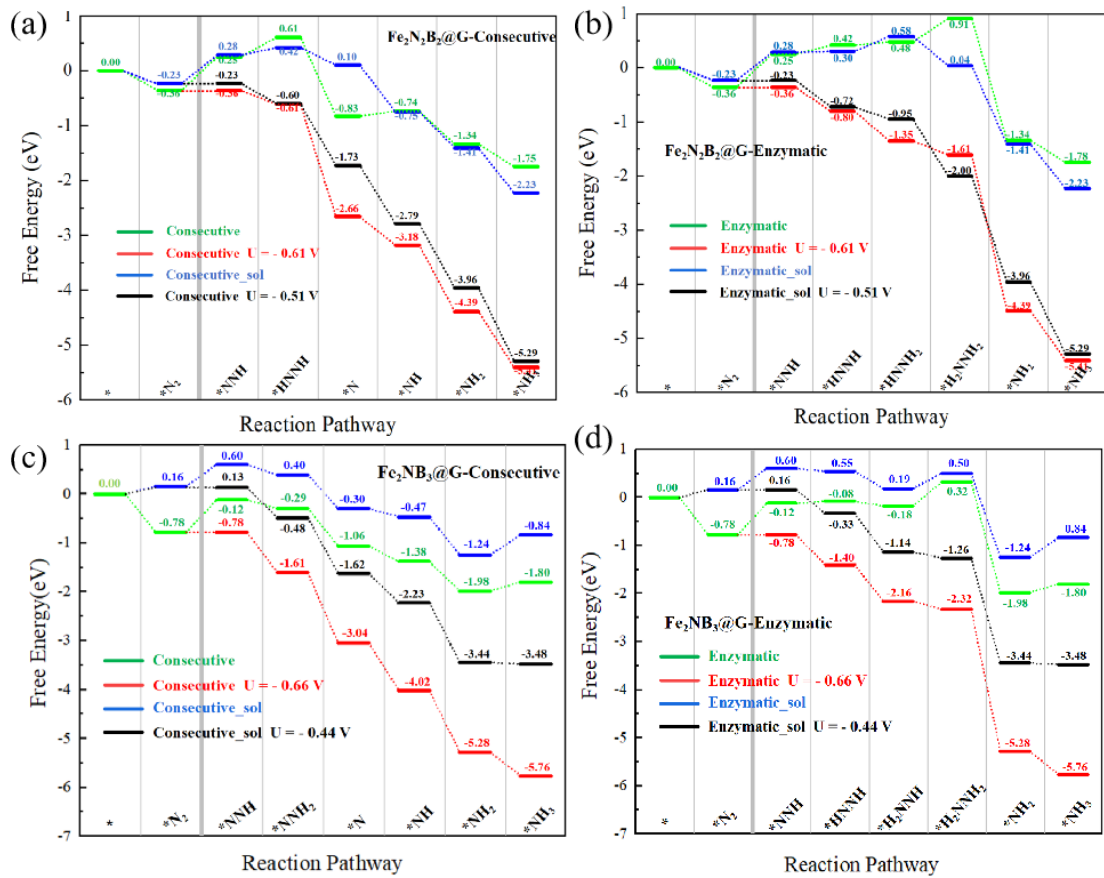


Figure S5. Free energy profiles of NRR on $\text{Fe}_2\text{N}_2\text{B}_2@\text{G}$ and $\text{Fe}_2\text{NB}_3@\text{G}$ catalyst considering solvation and applied potential effects.

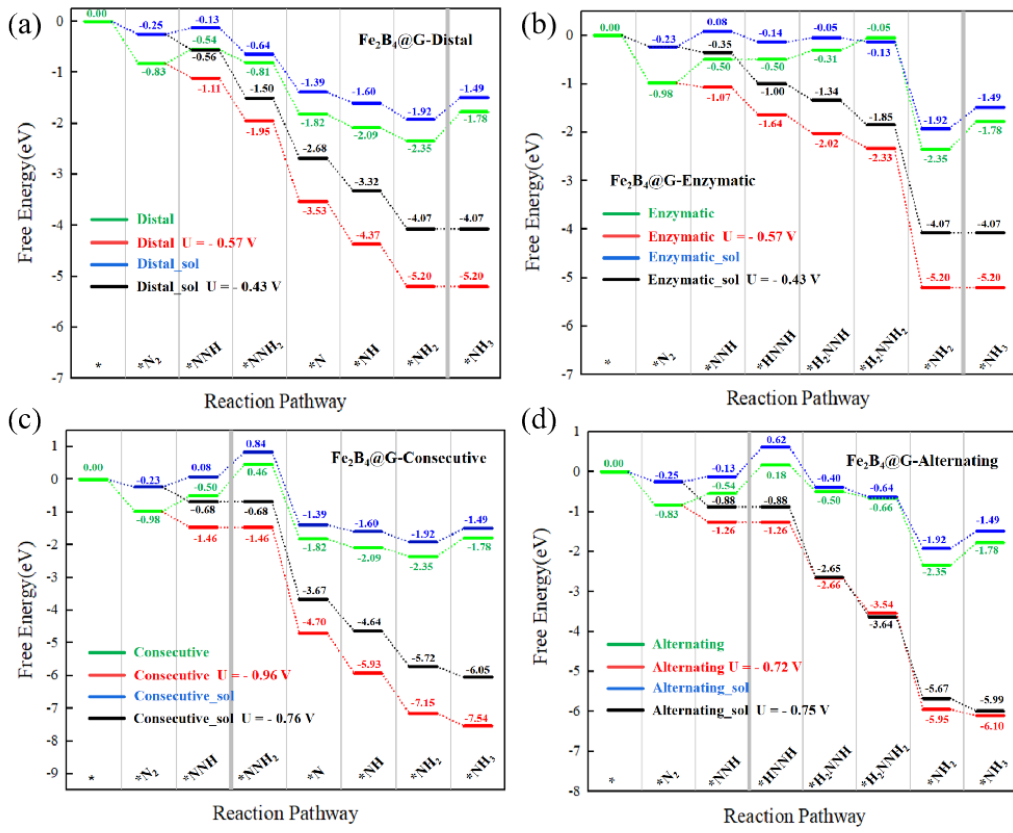


Figure S6. Free energy profiles of NRR on Fe₂B₄@G catalyst considering solvation and applied potential effects.

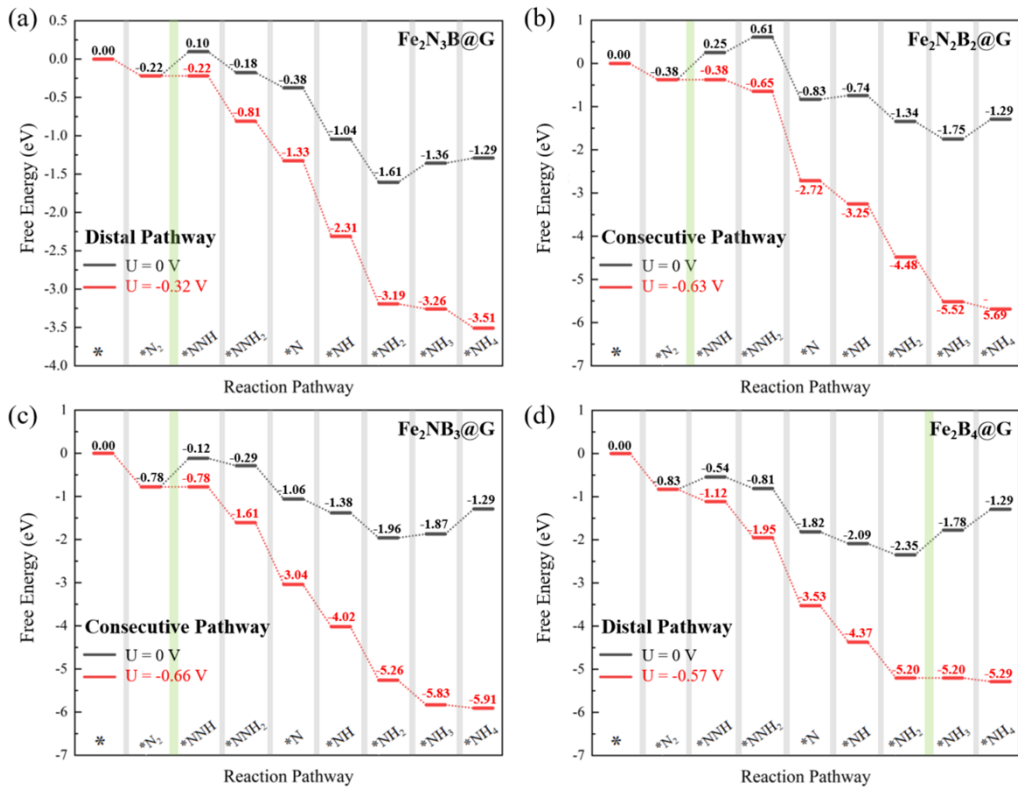


Figure S7. Free energy changes of the optimal reaction pathways for Fe₂N₃B@G, Fe₂N₂B₂@G, Fe₂NB₃@G, and Fe₂B₄@G catalysts. Each pathway is evaluated under different applied potentials,

showing the energy changes across the reaction steps and highlighting the most favorable pathways for nitrogen reduction.

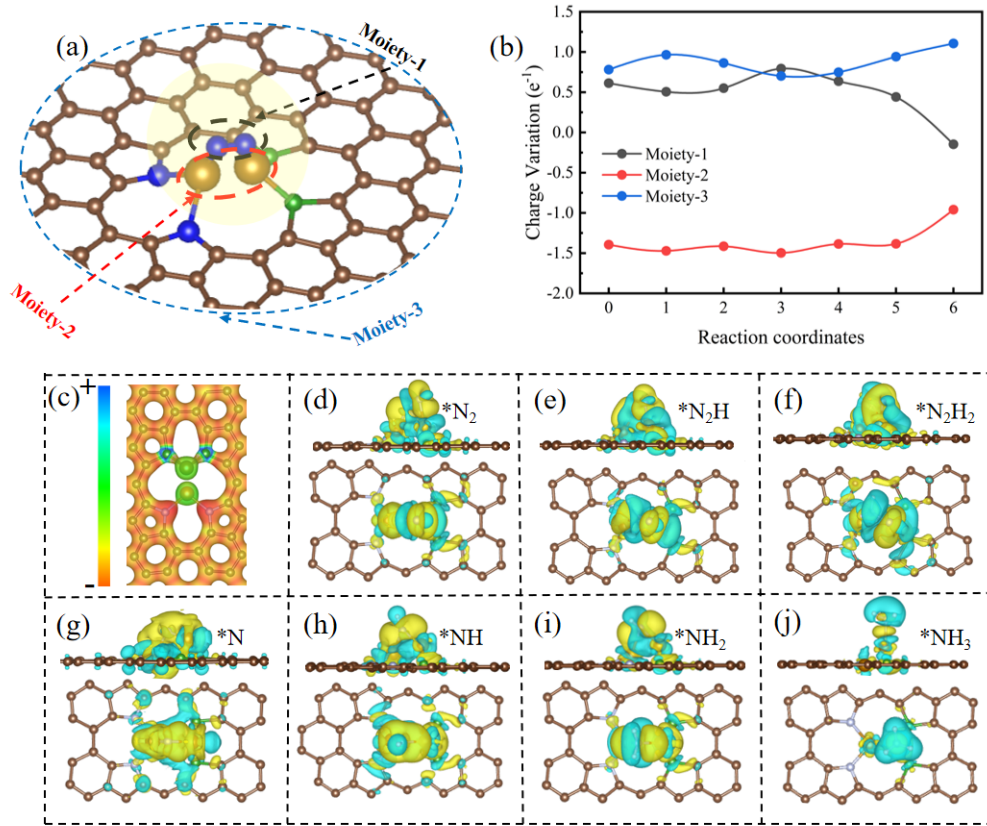


Figure S8. Electronic behavior and electrostatic potential distribution of consecutive pathway of $\text{Fe}_2\text{N}_2\text{B}_2@\text{G}$ catalyst in NRR. (a) Regional division of catalyst, Moiety-1 represents different reaction intermediates, Moiety-2 is dual-Fe site, and Moiety-3 represents the doped B and N region and its surrounding graphene network. (b) Changes in electron transfer. The horizontal axis corresponds to the different reaction stages in Figure R4 (d-j), showing the charge changes in different regions. (c) Electrostatic potential (ESP) diagram of $\text{Fe}_2\text{N}_2\text{B}_2@\text{G}$ catalyst, showing the enrichment of electrons at dual-Fe site. (d-j) Electron density distribution of different reaction intermediates on the catalyst surface, the yellow area indicates electron density accumulation, the cyan area indicates electron density removal, and the isosurface threshold is $0.001e/\text{Bohr}^3$.

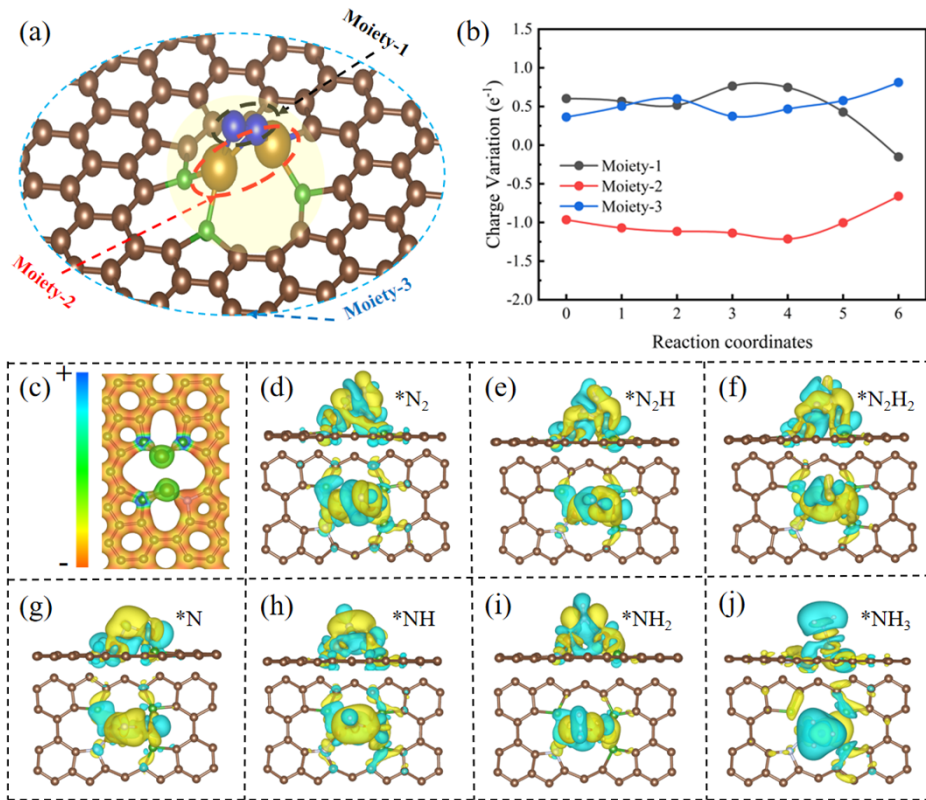


Figure S9. Electronic behavior and electrostatic potential distribution of consecutive pathway of $\text{Fe}_2\text{NB}_3@G$ catalyst in NRR.

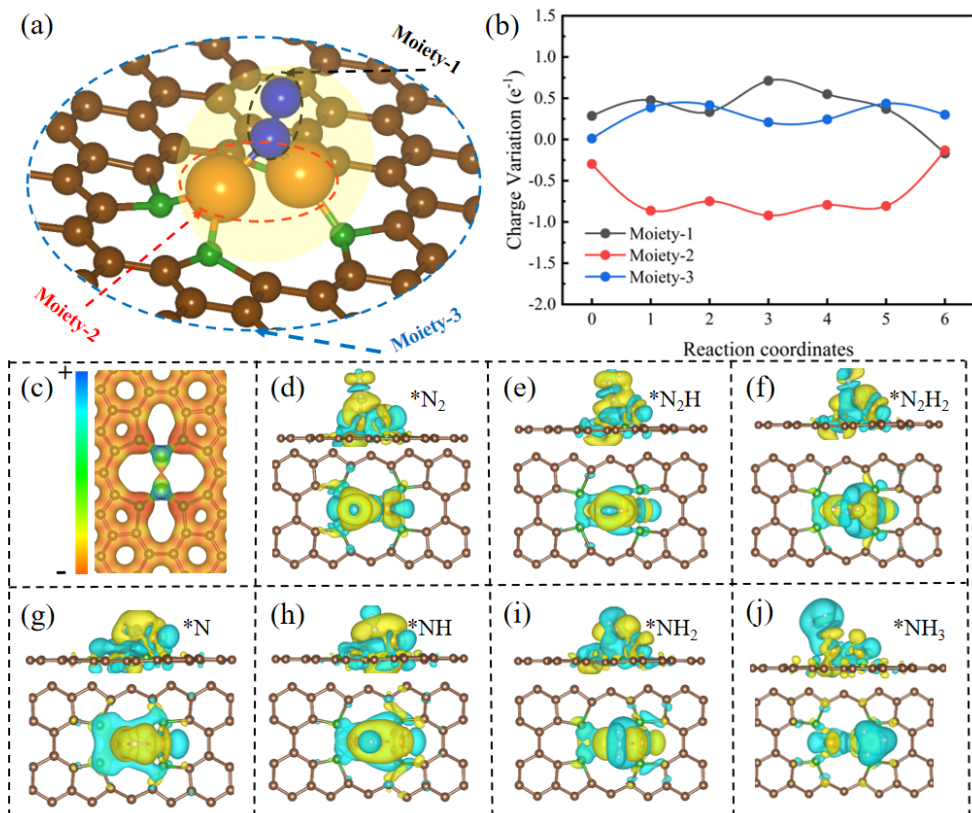


Figure S10. Electronic behavior and electrostatic potential distribution of consecutive pathway of $\text{Fe}_2\text{NB}_3@G$ catalyst in NRR.

$\text{Fe}_2\text{B}_4@\text{G}$ catalyst in NRR.

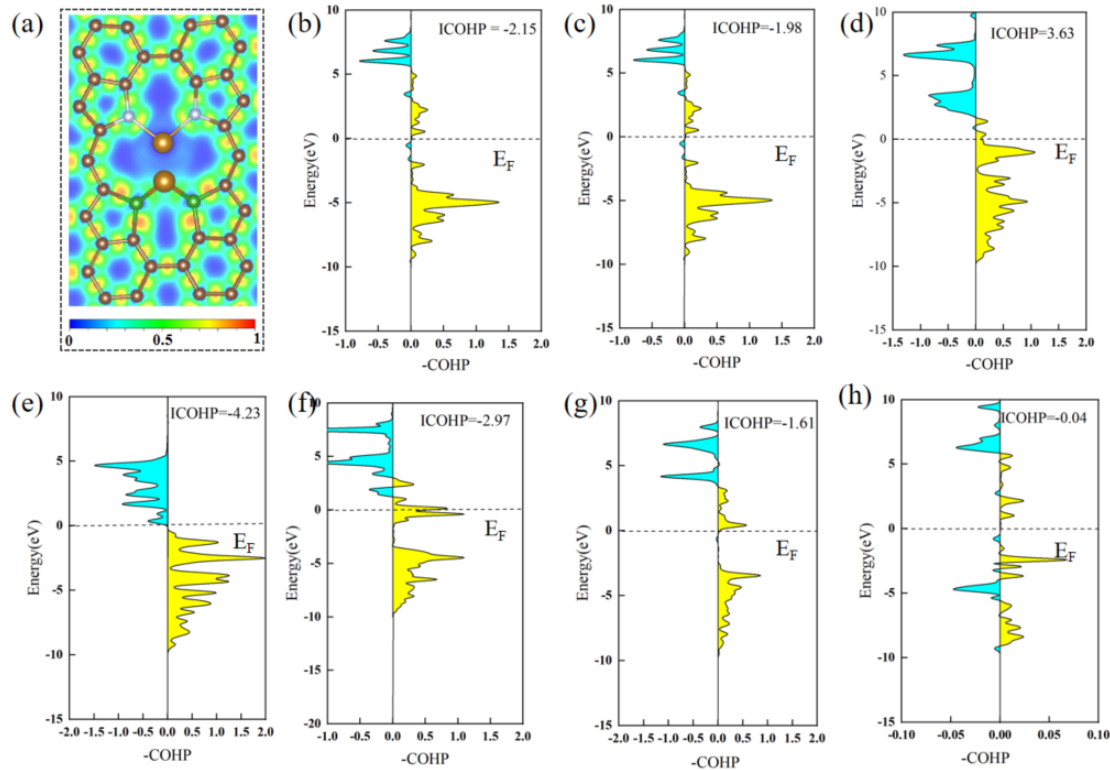


Figure S11. Electronic behavior for consecutive pathway of $\text{Fe}_2\text{N}_2\text{B}_2@\text{G}$ catalyst in NRR. (a) The electron localization function (ELF) of $\text{Fe}_2\text{N}_2\text{B}_2@\text{G}$ catalyst, the color represents the degree of electron localization, where the red area represents highly localized electron density and the blue area represents dispersed electron distribution. (b-h) The projected crystal orbital Hamiltonian population (COHP) between different reaction intermediates and Fe atoms in the distal pathway of the NRR for $\text{Fe}_2\text{N}_2\text{B}_2@\text{G}$ catalyst, the cyan and yellow areas represent the contributions of antibonding and bonding states, respectively.

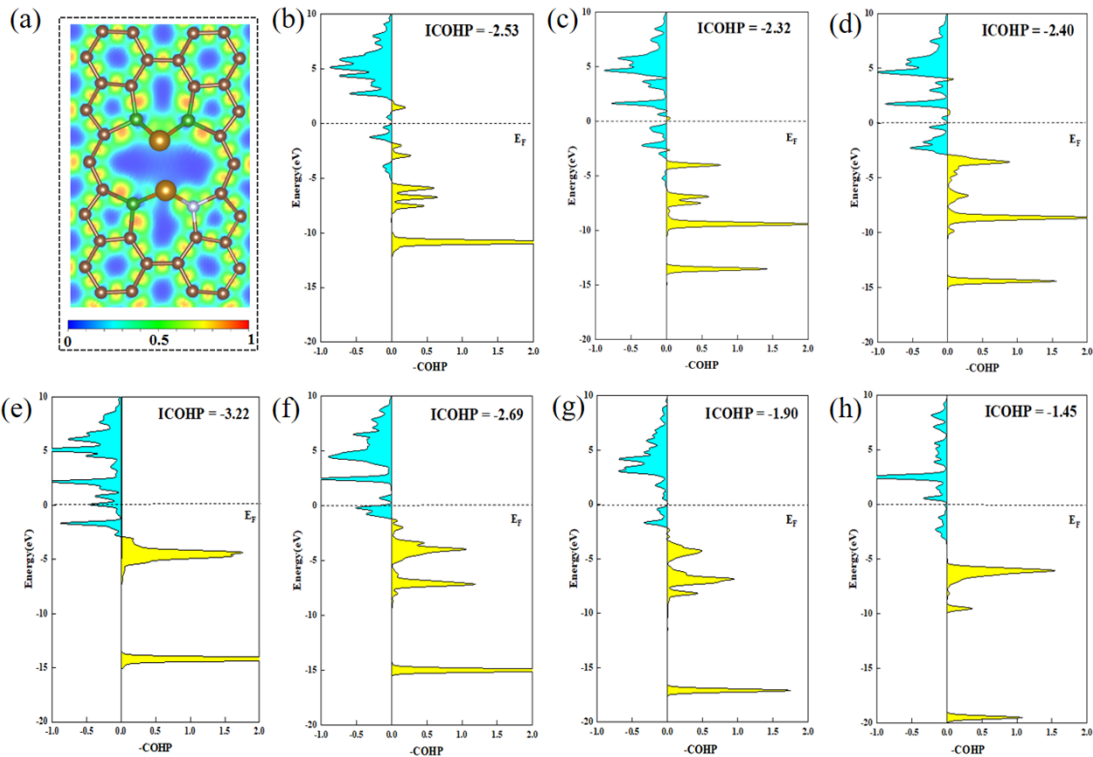


Figure S12. Electronic behavior for consecutive pathway of $\text{Fe}_2\text{Nb}_3@\text{G}$ in NRR.

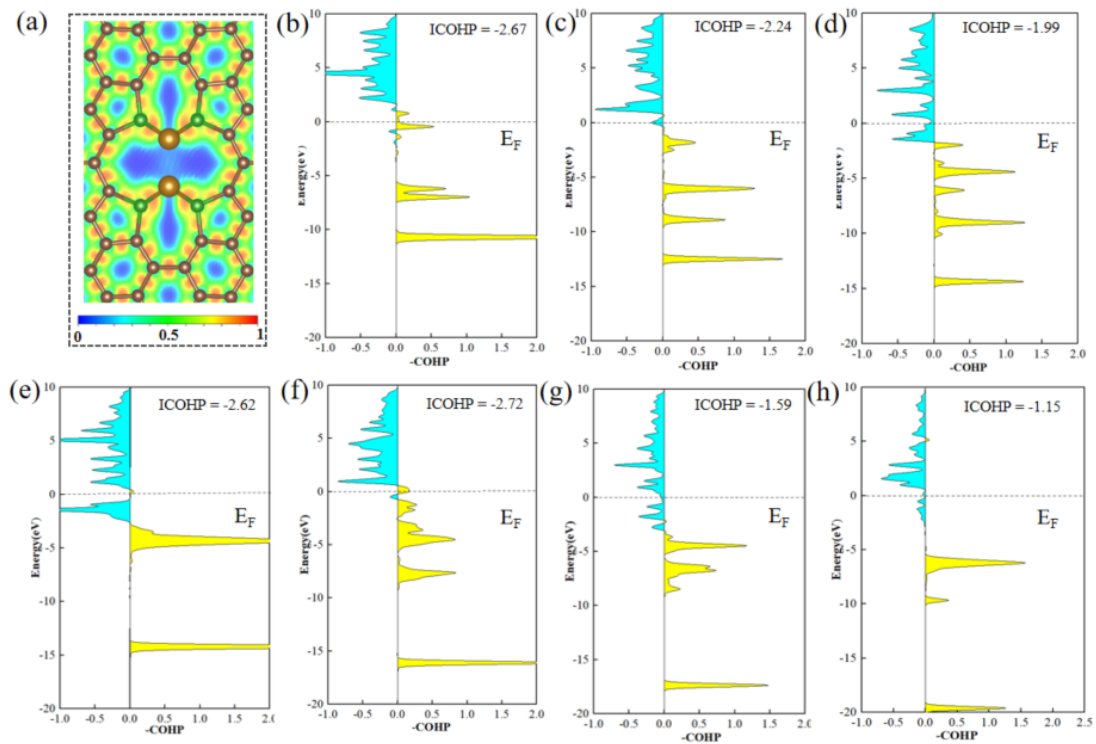


Figure S13. Electronic behavior for consecutive pathway of $\text{Fe}_2\text{Nb}_4@\text{G}$ catalyst in NRR.

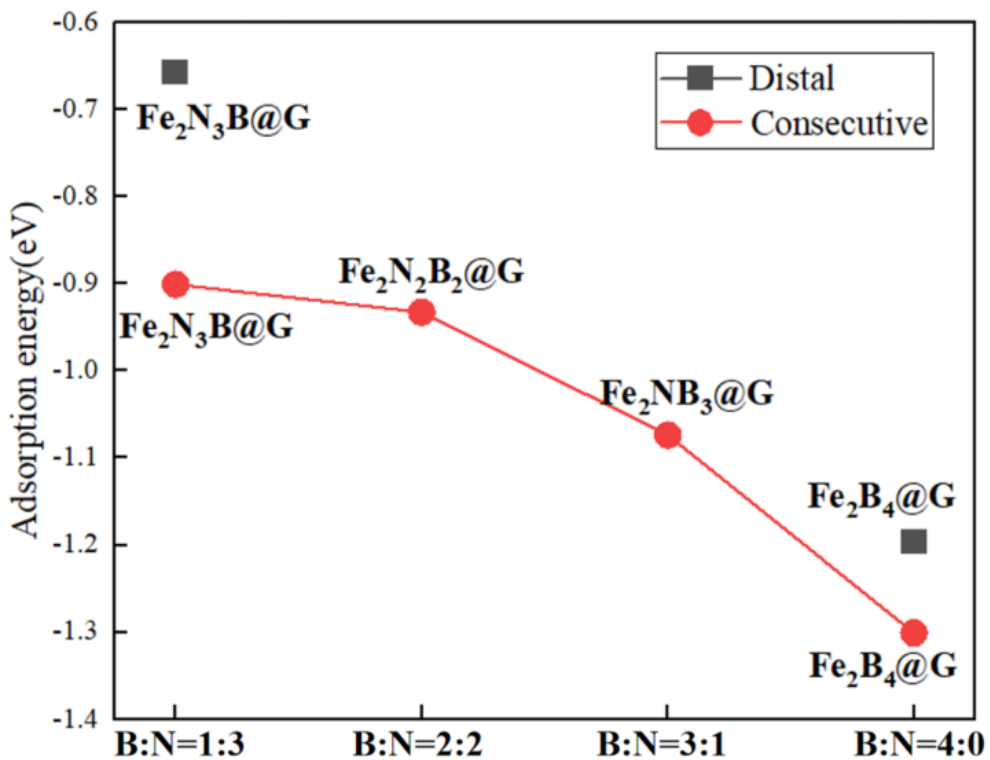


Figure S14. The calculated N_2 adsorption energy of $\text{Fe}_2\text{N}_x\text{B}_y@\text{G}$ catalysts with different B:N ratios. Red circles and black squares represent the consecutive and distal pathways, respectively.

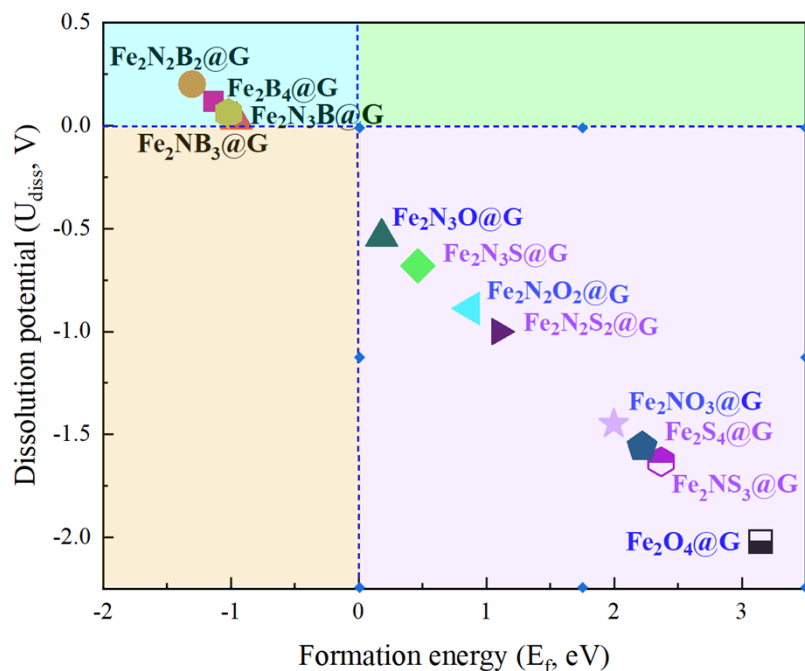


Figure S15. The formation energy and dissolution potential of Fe atoms on the $\text{Fe}_2\text{N}_x\text{B}_y@\text{G}$, $\text{Fe}_2\text{N}_x\text{O}_y@\text{G}$ and $\text{Fe}_2\text{N}_x\text{S}_y@\text{G}$ systems.

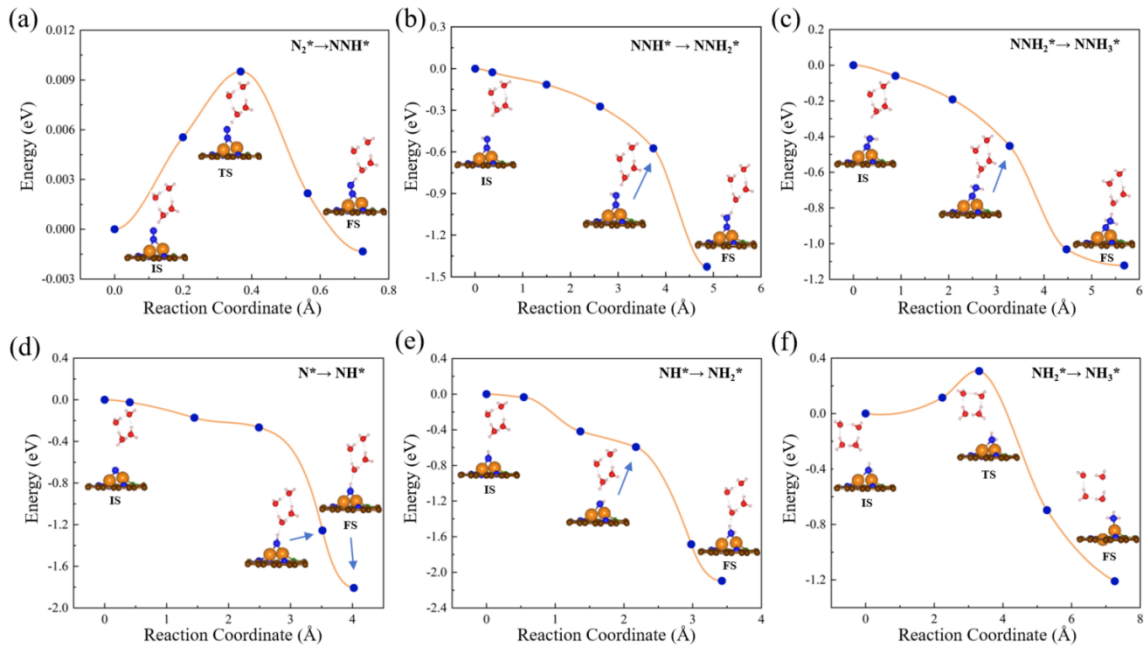


Figure S16. (a) – (b) Minimum energy pathways for NH_3 generation on $\text{Fe}_2\text{N}_3\text{B}@\text{G}$ catalyst: (a) $\text{N}_2^* \rightarrow \text{NNH}^*$, (b) $\text{NNH}^* \rightarrow \text{NNH}_2^*$, (c) $\text{NNH}_2^* \rightarrow \text{NH}^*$, (d) $\text{N}^* \rightarrow \text{NH}^*$, (e) $\text{NH}^* \rightarrow \text{NH}_2^*$, and (f) $\text{NH}_2^* \rightarrow \text{NH}_3^*$. The energy profiles are shown with respect to the reaction coordinate, with the initial state (IS), transition state (TS), and final state (FS) marked for each reaction step.

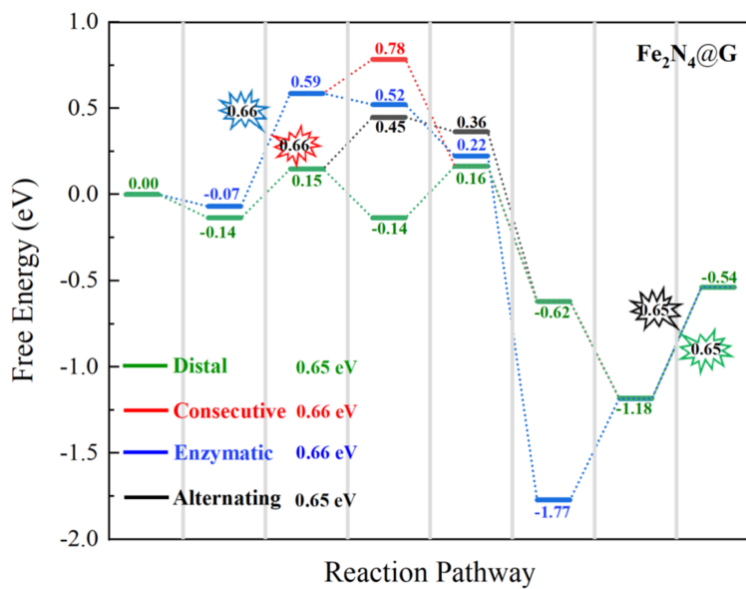


Figure S17. Free energy changes of the distal, alternating, consecutive and enzymatic pathways of NRR on $\text{Fe}_2\text{N}_4@\text{G}$. The free energy changes for key steps in all four pathways (distal, alternating, enzymatic, consecutive) are significantly higher than those of the B-doped $\text{Fe}_2\text{N}_3\text{B}@\text{G}$. This confirms that partial substitution of N with B helps regulate the electronic structure and enhances N_2 activation.